Advanced Radiation Panel design for applications in National Security and Food Safety

A. Bross[1], E.C. Dukes[2], S. Hansen[1], A. Pla-Dalmau[1], and P. Rubinov[1]

[1]Fermi National Accelerator Laboratory, Box 500, Batavia, IL 60510-5011, USA
[2]Physics Department, University of Virginia, Charlottesville, VA, USA

June 21, 2023

Abstract

We describe a new concept for a basic radiation detection panel based on conventional scintillator technology and commercially available solid-state photo-detectors. The panels are simple in construction, robust, very efficient and cost-effective and are easily scalable in size, from tens of cm^2 to tens of m^2. We describe two possible applications: flagging radioactive food coontamination and detection of illicit radio nucleides, such as those potentially used in a terrorist attack with a dirty bomb.

1 Overview

Fermilab is well positioned to make valuable contributions in the field of radiation detection. We:

1. Have in-depth understanding of the detector physics
2. Developed and defined the state-of-the-art in a number of relevant technological areas
3. Deployed many comprehensive readout systems
4. Have vast software and analysis experience
5. Have a well-developed system-integration methodology
6. And have fielded very-large-scale systems

One example is the technology developed for the Mu2e experiment at Fermilab.[1]. This experiment requires approximately 1200 m^2 of a very efficient detector for cosmic rays, and this technology can be extended to the radiation detection applications described here. The active element is the Di-counter unit (Figure 1) which consists of two extruded polystyrene-based scintillator counters with two holes for wavelength-shifting (WLS) fibers. The mechanical specifications for the Di-counter are given in Figure 2 A basic detector panel would consists of 3 "Di-counters", each up to 60 cm long. When a charged particle, such as a muon, passes through the scintillator, it loses energy and this energy is converted into blue light by the plastic scintillator. Similarly, if an Compton X-ray scatters in the plastic, the Compton electron produces light in the scintillator. Some of this blue light is absorbed by the WLS fiber and shifted into the green, where roughly 5% (in each direction) of the green-shifted light is piped along the fiber to a photo-detector. By using the WLS fibers to guide the light to the photo-detectors, it is possible to make large detectors with good light collection efficiency even when

This manuscript has been authored by Fermi Research Alliance, LLC under Contract No. DE-AC02-07CH11359 with the U.S. Department of Energy, Office of Science, Office of High Energy Physics.

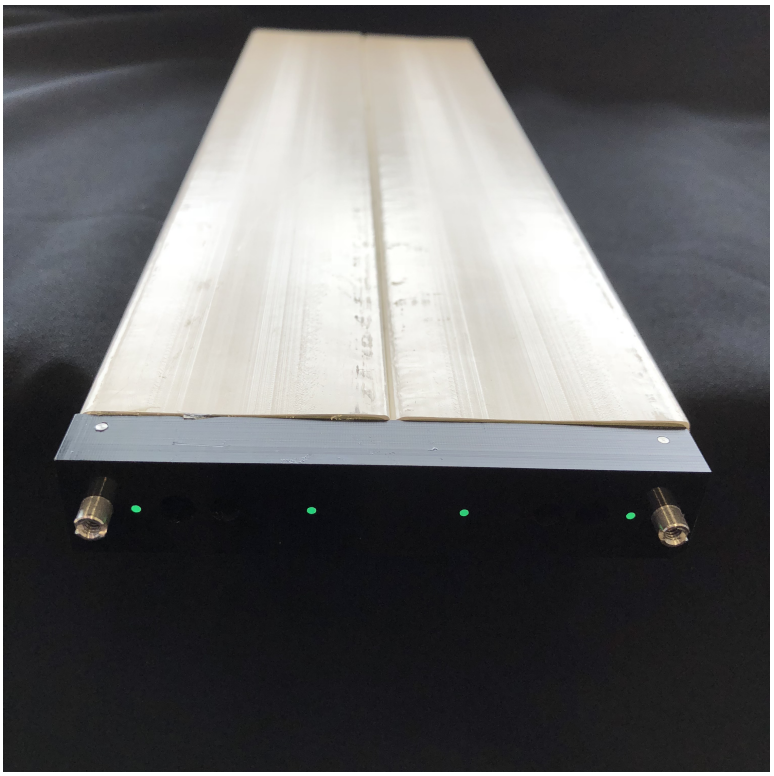

Figure 1: Photograph of a Di-counter.

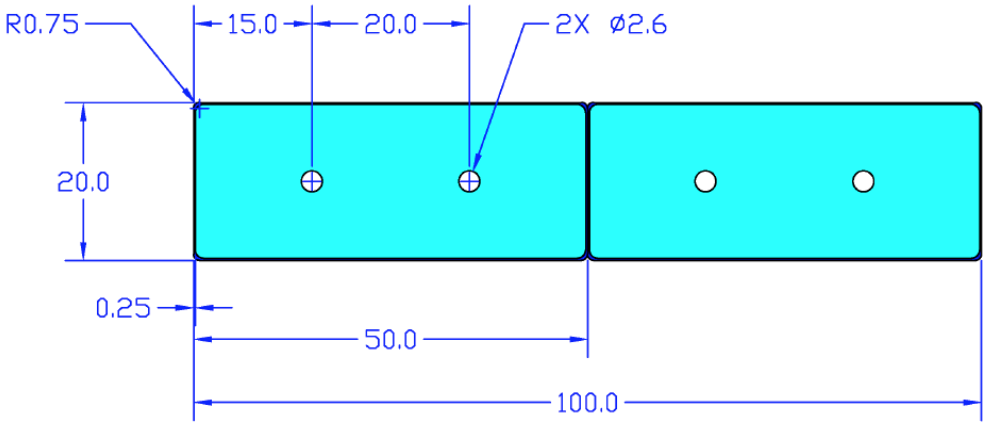

Figure 2: Nominal dimensions (mm) of a di-counter.

the particle hits far from the photo-detector. Figure 3 gives a schematic of this operating principle. The extrusions used for the project were fabricated in the FNAL-NICADD Extrusion Line Facility at Fermilab following the methodologies we have developed over the past 20 years. Figure 4a shows a photograph of a sample of the raw extrusion while Figure 4b shows a schematic of the full Di-counter assembly. The photo-detectors we use are silicon photomultipliers (SiPMs) [2]. Similar detectors are being used in several major particle physics experiments at high-energy physics laboratories throughout the world. A novel mechanical system was designed to align the fibers with the SiPMs which are carried on a consumer-grade PC board.

The photodetector system is modular in nature. An exploded view of the components is given in Figure 5. There are 4 SiPMs in each photodetector module with a module being mounted on both ends of the Di-counter, so that both ends of the WLS fiber are readout. The SiPM module carries 4 SiPMs

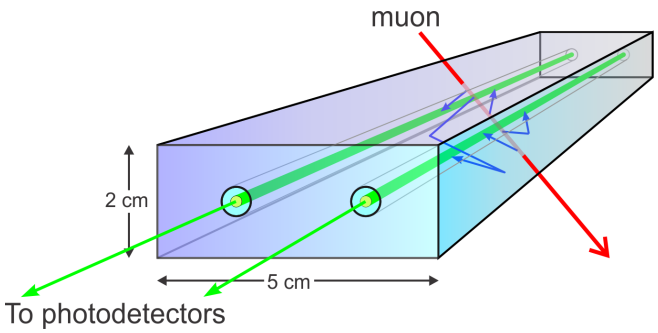

Figure 3: Detector operating principle

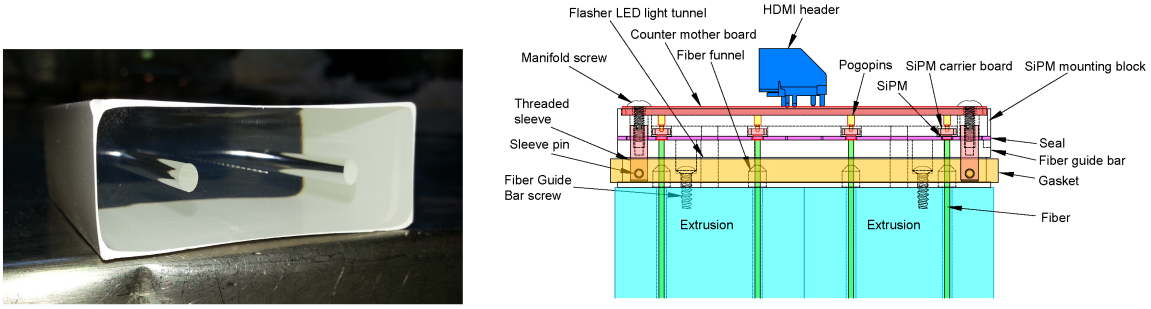

(a) Photograph of raw extrusion

(b) Schematic of the final Di-counter assembly

Figure 4: Extrusion and assembly details

that are 2 × 2 mm square. Figure 6 gives two photos of the module, a bottom view on the left showing the 4 SiPMs and a top view on the right showing the HDMI cable used for readout. The SiPM modules can easily be removed from the scintillator extrusions, so that they can be characterized separately. This allows to accurately set thresholds to remove the SiPM noise. An inexpensive readout system using commercial off-the-shelf parts, also designed for the Mu2e experiment, was used in the tests reported in this note.[3] We see two immediate applications for this technology. The first application

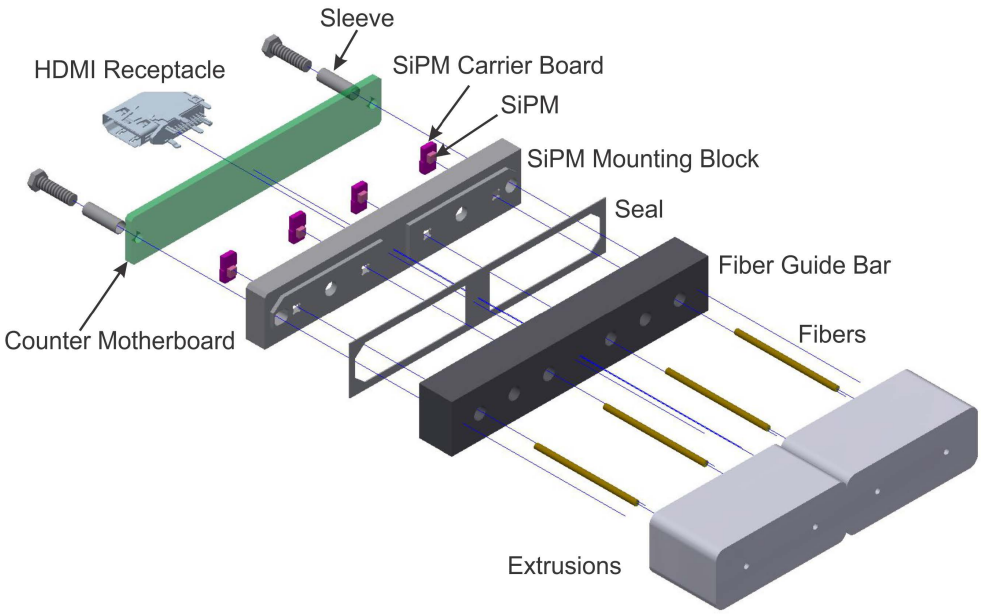

Figure 5: Exploded view of Di-counter readout module

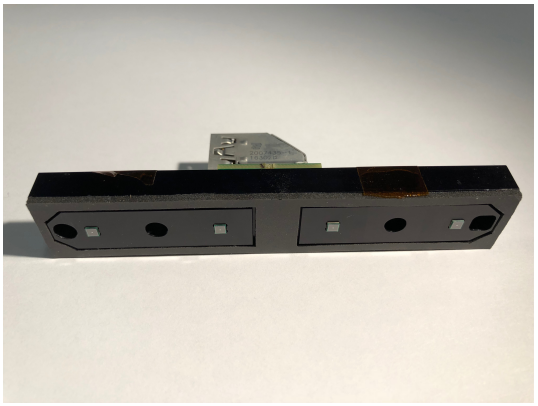

(a) SiPM module showing the 4 square SiPMs

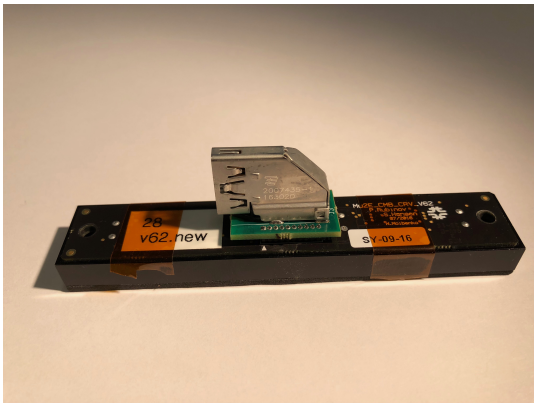

(b) SiPM module, top view

Figure 6: SiPM module

is for a radiation portal or urban-area monitors. These require a high sensitivity to a number of radionuclides such as, ^{109}Cd, ^{57}Co and ^{137}Cs. Neutron sensitivity can be provided by modifying the basic plate structure (see section 4). The second application is for food safety monitors. In areas where radioactive contamination of food products (primarily seafood) is a problem, we shall demonstrate that this technology can provide a high-sensitivity system that can flag unsafe seafood. It will provide an "in situ" background-subtracted counting environment that can quickly (within 10 sec.) flag unsafe food. Cosmic-ray interactions are easily rejected due to their very-large charge deposition and subsequent large electronic signal.

2 Results

Section 2.1 describes calibration of the detectors, section 2.2 describes the detector's performance for the detection of radioactive isotopes and section 2.3 presents data on the system's capabilities for flagging food contamination.

2.1 Calibration - ^{137}Cs

Because of the modularity of the detector (photo-detector module separate from scintillator detector), determining a threshold cut in ADC counts to remove the SiPM noise is very straightforward. The SiPM modules are removed from the scintillator, placed in a light-tight enclosure and data are then taken. An integration time of 10 seconds is used to produce histograms of the SiPM noise distribution. Figure 7 shows one such histogram for one counter in the Di-counter (sum of four SiPM signals). In order to effectively eliminate a large contribution from the SiPM noise, a cut in ADC counts is chosen to produce a summed SiPM noise rate of $\simeq$ 2 Hz.

The energy calibration is determined from the position of the ^{137}Cs Compton edge in ADC counts. A 0.6μCi ^{137}Cs source is placed in direct contact with one of the counters in the di-counter. A 10 second integration is performed and the sum of the output from the 4 SiPMs that readout the 4 WLS fiber ends in the counter are histogrammed. The system gain is set so that the Compton edge is at $\simeq$ 500 ADC counts. A typical distribution is shown in Figure 8. The Compton edge gives us the equivalent energy deposition per ADC count, since we know that the energy of the Compton edge is determined from:

$$E_{Compton} = E(1 - \frac{1}{1 + \frac{2E}{m_e c^2}}) \quad (1)$$

where E is the ^{137}Cs photopeak energy (662 keV). The Compton edge is thus at $\simeq$ 480 keV. From Figure 8 we see that the Compton edge is at $\simeq$ bin 515. The pedestal is at bin 15 (see Figure 7), so the

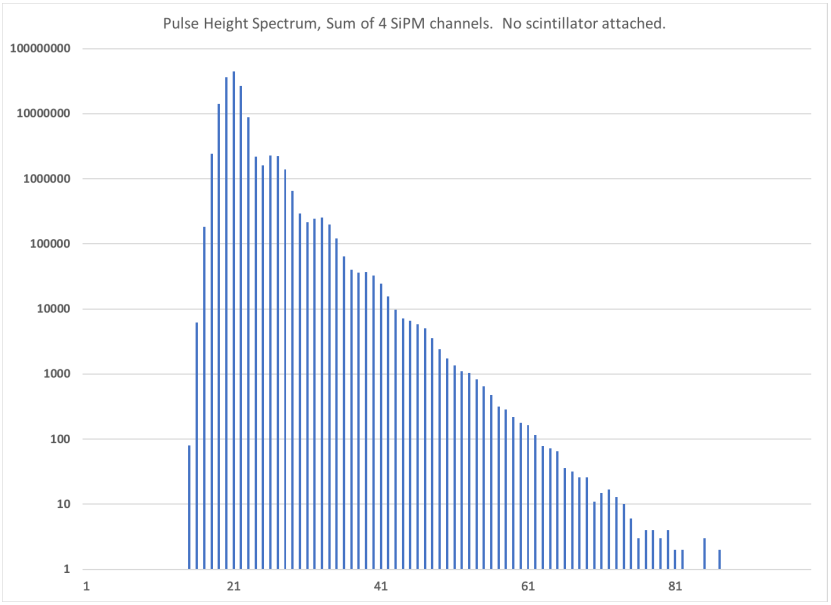

Figure 7: Noise histogram for sum of 4 SiPMs

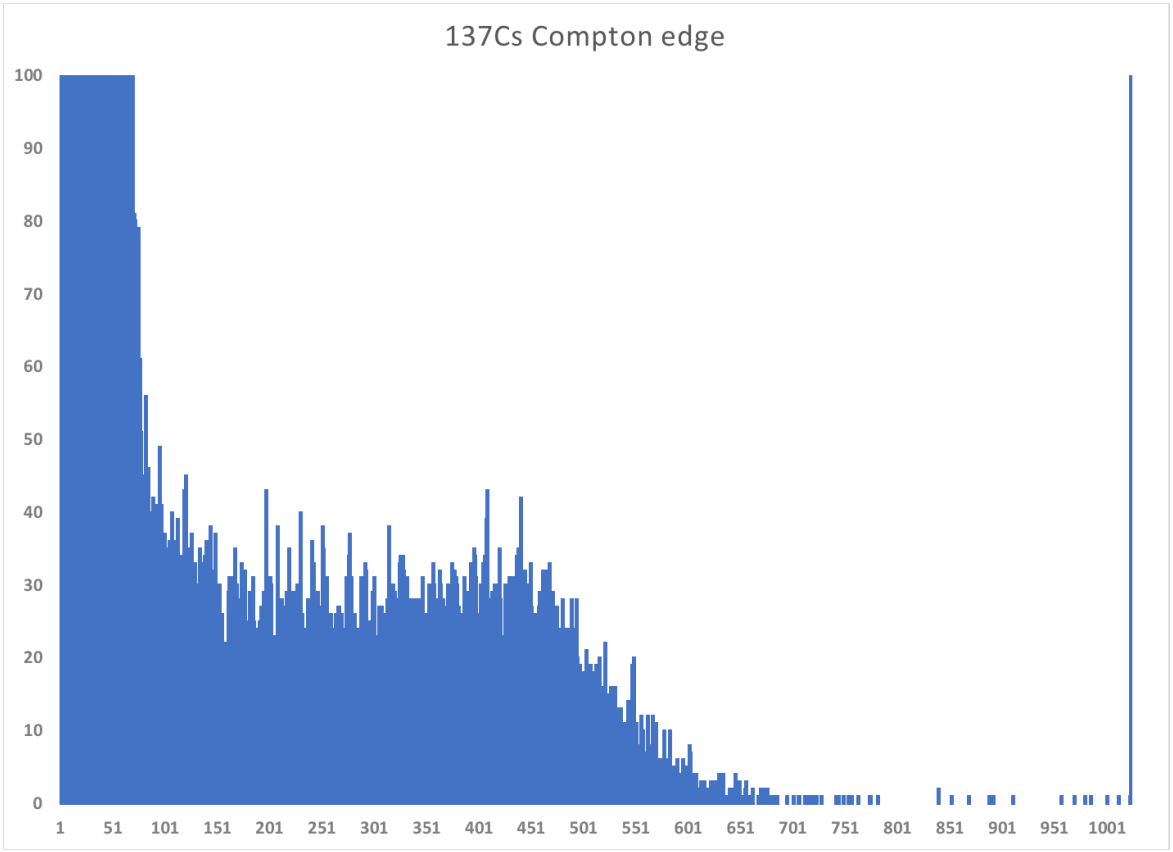

Figure 8: ^{137}Cs signal (source distance = 0) from the sum of 4 SiPMs on one counter

energy per bin is equal to 480/(515-15) $\simeq$ 1 keV per bin. The overflow bin shown in Figure 8 captures most of the cosmic-ray muon events. However, we also see a few hits between the Compton edge and the overflow bin that are likely due to cosmic-ray muons that just graze the corner of the counter.

2.2 Data with ^{137}Cs source

The data described in this section used the same 0.6μCi ^{137}Cs source that was used for calibration in Section 2.1. First data are taken without the source in place and then data are taken with the source positioned 30 cm above one of the counters in the Di-counter. Data taken without the source, gives us the terrestrial background rate in our laboratory.

2.2.1 Di-Counter with 1.4mm WLS fiber

These tests used a Di-counter that was assembled with 1.4mm WLS fiber. In addition, for this sample, glue (BC600) was used to fill the holes in the extrusion that hold the WLS fiber. This improves the optical coupling between the bulk scintillation in the extrusion and the WLS fiber. The background (no source) data are shown in Figure 9. For the measurement, an ADC cut at 77 yielded the best results. The count rate was 391 for a 10 second integration with no source in place. Figure 10 shows data with the ^{137}Cs source positioned 30 cm above the counter. In this case, the count rate is 696 for a 10 second integration. The differential count rate (with source-without source) was $\simeq$ 31 Hz. Using

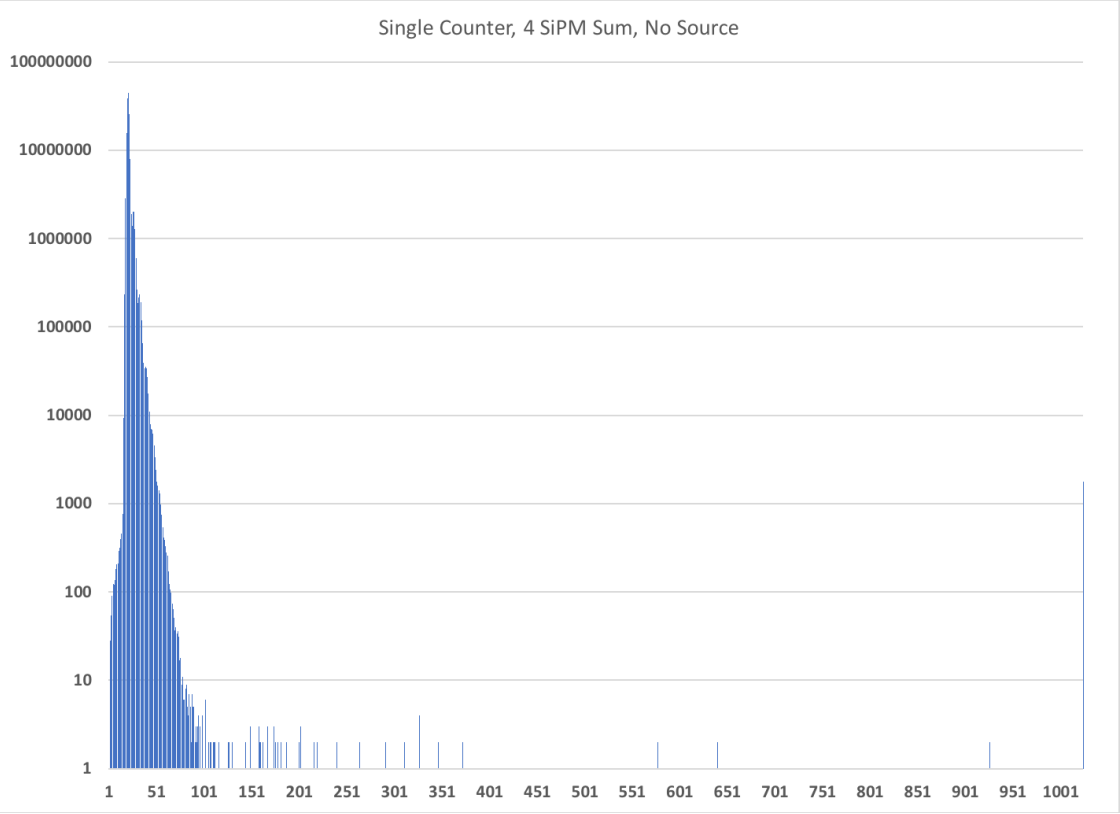

Figure 9: 10 second integration of signal from 1 counter, no source present

the source strength (0.6μCi), source distance (30 cm), the counter area and thickness (30 cm $\times$ 5cm $\times$ 2 cm thick) and the stopping power of polystyrene at 662 keV, for full efficiency, we would expect a count rate of 43Hz. Therefore, this counter, as configured, is $\simeq$ 70% efficient for the detection ^{137}Cs gammas that interact in the scintillator. As a cross check, for the data with no source, we integrated the flux above the ADC cut of 77, weighted by 1 keV per bin to obtain a total integrated dose for the 10 second exposure. Assuming a 70% efficiency also for the background gammas and extrapolating for a 1 year exposure, we obtain $\simeq$ 25 mrem, which is consistent with terrestrial background rates. Remember, cosmic-ray counts (overflow bin) are not included and account for $\simeq$ half the total yearly dose rate at sea level.

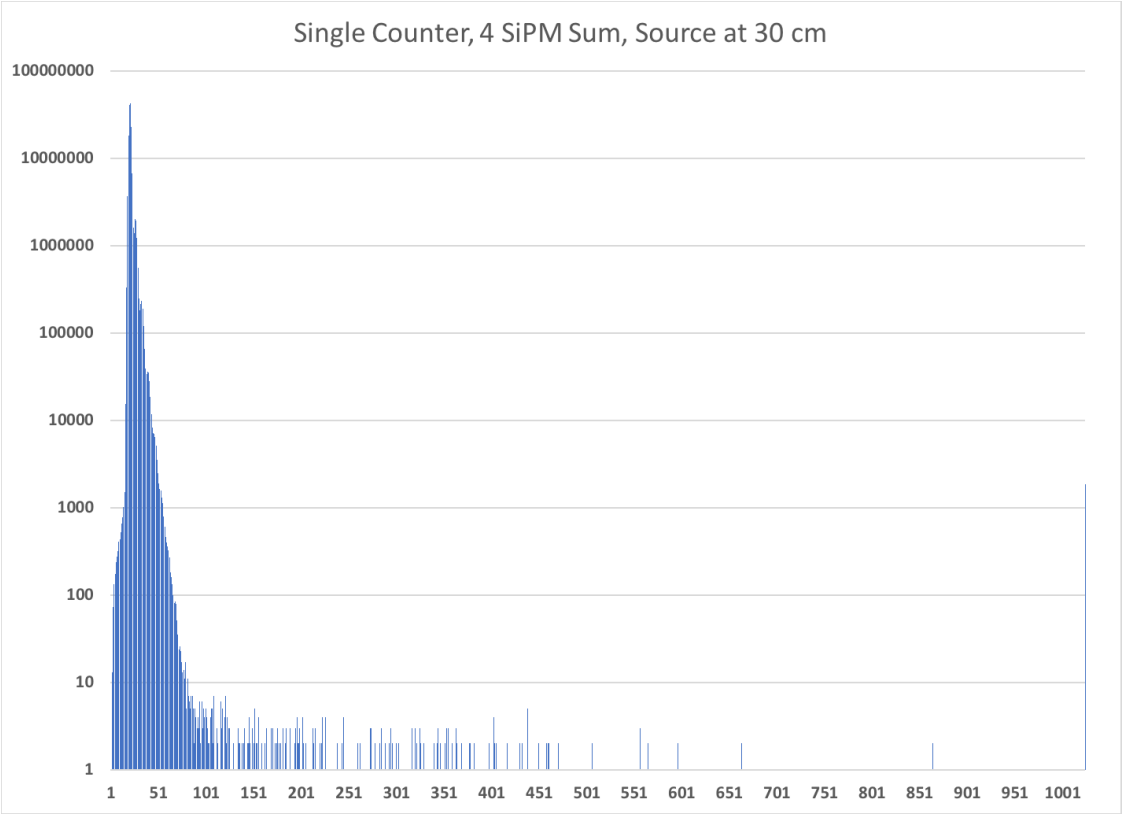

Figure 10: 10 second integration of signal from 1 counter, source 30 cm from counter

We have tested this counter's performance against a commercial standard – a Bicron Analyst. Table 1 gives the results. In each case, the system's sensitivity to our ^{137}Cs source was measured. σ is the $\sqrt{Bkg}$. As can be seen in Table 1, our panel out performs the commercial standard which uses an

Table 1: Commercial device comparison

Device	T(sec)	Dist.(cm)	S	Bkg	S-Bkg(Hz)	σ=SQRT(Bkg)	No. σ above Bkg
$\frac{1}{2}$ Di-Counter	10	30	696	391	30.5	19.8	16
Bicron Analyst	10	30	327	217	11	15	7

expensive NaI crystal for its detector.

Extrapolating our panel performance described above to the DHS portal spec for ^{137}Cs (100 cps/μCi for 47k cm^3 of plastic detector at a distance of 2m), we have an equivalent count rate of $\simeq$ 1200 Hz above background – **more than 12X** the portal specification.

2.3 Food safety monitoring test

In order to study food safety applications for our detector, we have used our prototype panel to measure the count rate for 100 grams of Brazil nuts, which have a nominal activity of 10 Bq. Food safety standards in the US use a limit of 1000 Bq/kg, but in the Far East, in part in reaction to illegal fishing after the Fukashima accident, the standards are stricter, and food is deemed safe if the activity is less than 100 Bq/kg. In our tests, we evenly spread the 100 grams of Brazil nuts directly on top of one counter of a Di-counter. The measured signal due to the activity of the nuts was $\simeq$ 3 Hz. In this study, we found that the optimal (best signal over background) was achieved with an ADC of 190, which is significantly higher than that needed to reduce the SiPM noise to 2 Hz. The Di-Counter data in Table 2 were obtained using this ADC cut. We also used the Bicron Analyst to detect the radiation from the nuts. In this case, our panel performs much better than the NaI-based

Table 2: Sensitivity to Food radioactivity

Device	T(sec)	Rate, "food" on	Rate, "food" off	Delta (Hz)	No. σ
$\frac{1}{2}$ Di-Counter	10	102	70	3	3.8
Bicron Analyst	10	137	131	0.6	0.5

detector. This is due to the large surface area (relative to the Bicron Analyst's NaI crystal) of our counter, which results in much better effective stopping efficiency for the radiation. In a practical installation at point-of-purchase, the sensitive area of the radiation panel would be roughly 30 cm $\times$ 30 cm or roughly 6 times the area of the single counter of a Di-counter used in the test described above. The background rate would, therefore, increase by 6, reaching $\simeq$ 420 counts in our 10 sec integration window. One sigma above background would be 20 counts. For a 1kg sample with 100Bq of radioactive contamination placed on this 30 cm $\times$ 30 cm counter and based on the results given above, we would have a count above background of 300 counts (30 Hz $\times$ 10 sec.) or $\simeq 15\sigma$ above background. This case clearly demonstrates the efficacy of our technology for flagging, with very-high efficiency and very-low false-positive rate, food borne radioactive contamination at the 100 Bq/kg level.

3 Real-world example

Another possible application for this technology would be to protect large areas from illicit radiation sources such as might be used in a "dirty bomb" attack by terrorists. Here we give an idea of how an array of counters *(Radiation Cell Towers)* with the type of performance we demonstrated above for ^{137}Cs could be used to cover a city. As an example, we use the NY borough of Manhattan. See Figure 11. Manhattan has a total area of $\simeq$ 60 km^2. We assume the performance level indicated above and extend the area of each panel to 60 cm $\times$ 30 cm (still small and easily deployable on light poles, for example). The metric we use here is the detection of the equivalent of an unshielded 10mCi ^{137}Cs source. This would be equivalent to approximately 6 cm of lead surrounding a 10kCi source. Table 3 summarizes the performance of this 60 cm $\times$ 30 cm detector panel extrapolated from the measured detector performance described in section 2.2. A single panel can detect 10 mCi of un-shielded ^{137}Cs

Table 3: Radiation Cell Towers counter performance

Device	Int. time (sec)	Bkg	$\sigma = \sqrt{}$(Bkg.)	Dist.(m) when signal is 3σ above Bkg.
60X30 cm Counter	10	4700	69	163

at a distance of 163 m, assuming a ten second integration window. A single panel can cover an area of approximately 0.084 km^2 based on this number. In addition, we are only considering half the solid angle here in order to be conservative. In a real deployment, the panels would obviously be sensitive to radiation coming from all angles. Therefore, $\simeq$ 720 such panels could monitor the entire borough

Figure 11: Map of Manhattan.

of Manhattan. To fully engineer an environmentally robust detector would require $\simeq$ \$10M in non-recurring engineering costs. Once in production, we estimate a unit cost of $\simeq$\$2000 with installation and infrastructure costs of \$3000 per unit, averaged over the entire system. Total investment is then on the order of \$13.3M including non-recurring engineering (NRE). A more detailed cost breakdown is given in Table 4.

Table 4: Cost Model

Component	**Number**	**Cost (\$)**	**Total (k\$)**
Mechanical engineering (NRE)	Lot	-	3000
Electrical engineering (NRE)	Lot	-	5000
Software engineering (NRE)	Lot	-	2000
Scintillator	720	72	52
Fiber	17280	1	18
Photodetector module	17280	5	86
Electronics	17280	20	346
Enclosure	720	350	252
Assembly and test	720	500	360
Installation	720	3000	2160
TOTAL			**13274**

4 Neutron sensitivity enhancement

Although scintillator detectors have sensitivity to fast neutrons, it is difficult to distinguish a neutron event from ordinary ionization radiation. In addition, plastic scintillator has very little sensitivity to thermal neutrons. The extruded plastic scintillator technology that has been developed at Fermilab can be extended to produce a neutron sensitive plastic and, if there is an argument for neutron sensitivity also, a second panel could be added to our system to include this capability.

An extruded scintillator that is only sensitive to thermal neutrons, based on our existing technology, could be developed and put into the field. This would be of particular benefit in aiding in the detection of weapons-grade plutonium (WGPu). The basic idea is to prepare polystyrene-based scintillator with ^{6}LiF nano-particles and detect neutrons via the process: n + ^{6}Li $\rightarrow$ ^{7}Li* $\rightarrow$ ^{4}He + ^{3}H + 4.79 MeV. The daughter particles in the reaction (α + triton) deposit all their energy in a very thin layer ($\simeq$ 50 μm). In this way, a thin active layer can efficiently detect neutrons, where gammas and minimum ionizing

particles would deposit very little energy and their signal would fall below threshold. The thin layer would be coupled to a non-scintillating plate which would wavelength shift the light from the neutron detection reaction. This light would be trapped in this plate and the light would be readout as described above. Our extrusion process lends itself in a very natural way to producing the needed plates.

5 Discussion

We have shown in this note that modern plastic-scintillator technology using solid-state light detectors, that has been developed for high-energy physics applications, can find far-reaching use in national security and food safety applications. There is still room for increased performance levels through detector optimization studies, but most of the underlying technology base is firmly in place. The cost–performance envelope for these types of systems is also very attractive.

6 Conclusions

Our demo radiation detection panel, when extrapolated to the needs of the two applications described above, meets or exceeds their specification requirements. For radiation detection security applications, our system has a sensitivity 12X the DHS minimum specification. For food safety, we have shown that our technology can meet the 100 Bq/kg specification used in Asia, which is 10X lower than that used in the US. The technology we have developed for HEP applications, when properly configured, is likely to be able to significantly surpass industry specifications, while being both cost effective and mechanically robust. Directed R&D can improve performance even further.

References

[1] Mu2e collaboration, R. Donghia, *The Mu2e experiment at Fermilab: Design and status*, *Nuovo Cim.* **C40** (2018) 176.

[2] B. Beischer, R. Greim, T. Kirn, C. Mai, G. Roper Yearwood, S. Schael et al., *The development of a high-resolution scintillating fiber tracker with silicon photomultiplier readout*, *Nucl. Instrum. Meth.* **A628** (2011) 403–406.

[3] Mu2e collaboration, A. Artikov et al., *Photoelectron Yields of Scintillation Counters with Embedded Wavelength-Shifting Fibers Read Out With Silicon Photomultipliers*, *Nucl. Instrum. Meth.* **A890** (2018) 84–95, [1709.06587].